Two-Dimensional Glide-Symmetric Dielectric Structures for Planar Graded-Index Lens Antennas

J.-M. Poyanco, O. Zetterstrom, *Student Member, IEEE*, P. Castillo-Tapia, *Student Member, IEEE*, N. J. G. Fonseca, *Senior Member, IEEE*, F. Pizarro, *Member, IEEE*, O. Quevedo-Teruel, *Senior Member, IEEE*

***Abstract*—In this letter, we propose and study a two-dimensional glide-symmetric dielectric periodic structure. We demonstrate that glide symmetry broadens the bandwidth of operation and achieves lower effective refractive indices when compared to non-glide configurations. These two properties are beneficial for producing graded-index lens antennas. To demonstrate the potential of the proposed unit cell, we designed a Luneburg lens operating in the K- and K_a-bands. The lens was manufactured with conventional additive manufacturing and it has a potential use for future wireless communications given its low-cost and low-profile.**

***Index Terms*—Glide symmetry, Luneburg lens, dielectric lens antennas, additive manufacturing.**

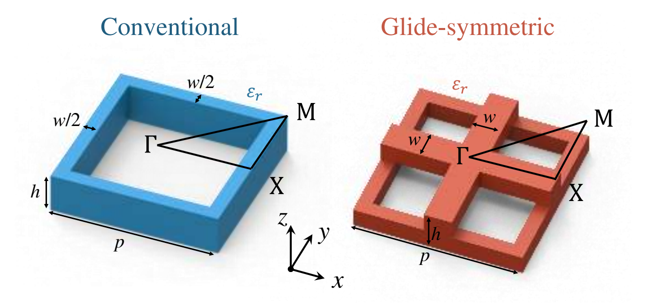

Fig. 1. Configuration and design parameters of two-dimensional dielectric unit cells, conventional and glide-symmetric.

I. Introduction

A periodic structure is glide-symmetric if it is invariant after a translation and a mirroring operation [1], [2]. The properties of these periodic structures were first studied for one-dimensional configurations in the 1960s and 1970s [3], [4]. Recently, the electromagnetic properties of two-dimensional (2D) glide-symmetric structures have been investigated and a number of benefits have been discovered [5]. For example, it has been demonstrated that glide symmetry broadens the bandwidth of the electromagnetic band gaps (EBGs) in holey periodic structures [6]. This property has been applied to produce cost-effective gap-waveguide components [7], [8], flanges with low-leakage [9], [10], and filters [11]. Glide symmetry also increases the level of anisotropy of periodic structures [12], [13], which can be used, for example, to compress the size of lenses with transformation optics [14], [15]. Furthermore, glide symmetry enhances the magnetic response of holey periodic structures. This feature can be used to reduce the reflections in the transitions between dielectric materials [16].

Another relevant quality of glide symmetry is that it increases the equivalent refractive index of periodic structures and its bandwidth [17], [18]. These features were used to produce broadband 2D lenses [19]–[21] and artificial materials [22], [23]. For example, in [21], glide symmetry was proposed to produce a Maxwell fish-eye lens in printed technology. In [19], [20], glide symmetry was used to produce fully metallic graded-index lens antennas. In [19], the lens was implemented with glide-symmetric holes; while in [20], the lens was designed with glide-symmetric pins.

When considering fully dielectric glide-symmetric structures, very few configurations have been studied. In [24], the authors studied the propagation constant in a dielectric layer surrounded by corrugated dielectric slabs possessing glide symmetry. In [25], cylindrical glide-symmetric holes were employed to produce a three-dimensional optically transformed Luneburg lens.

In this letter, we propose and study (including a multimodal analysis) a 2D glide-symmetric periodic structure that is fully dielectric and can be manufactured using a conventional 3D-printer. The advantages exhibited with respect to non-glide configurations are the reduction of the minimum achievable effective refractive index, increased isotropy, and increased bandwidth of operation. These properties are beneficial for the implementation of dielectric graded-index lenses. Here, we demonstrate the potential use of this unit cell with the design and implementation of a 2D Luneburg lens antenna operating in the K- and K_a bands, providing a low-cost low-profile alternative to the reported planar lens designs at those frequencies [19], [20], [26]–[31].

II. 2D Dielectric Unit Cell

In this section, two 2D-periodic dielectric structures (with and without glide symmetry) are analyzed and compared. The unit cells of these periodic structures are represented in Fig. 1. The structures are periodic in the *xy*-plane and are placed in a

This work has been partly funded by the strategic innovation program Smarter Electronics System - a joint venture of Vinnova, Formas and the Swedish Energy Agency, under project High-Int (2019-02103). The work of O. Quevedo-Teruel and P. Castillo-Tapia was also funded by the VR Project 2019-03933 under call ”Research project grant within natural and engineering sciences”. The work of O. Zetterstrom was funded by the ESA ARTES contract 4000125905/18/NL. The work of J.M. Poyanco and F. Pizarro was founded by the Chilean project ANID PCI-MEC 8019007.

J.-M. Poyanco and F. Pizarro are with the Pontificia Universidad Católica de Valparaíso, Escuela de Ingeniería Electrica, 2362804,Valparaiso, Chile (e-mails: jose-manuel.poyanco.a@mail.pucv.cl; francisco.pizarro.t@pucv.cl

O. Zetterstrom, P. Castillo-Tapia and O. Quevedo-Teruel are with the Division of Electromagnetic Engineering, KTH Royal Institute of Technology, SE-100 44 Stockholm, Sweden (e-mails: oskarz@kth.se; pilarct@kth.se; oscarqt@kth.se).

N. J. G. Fonseca is with the Antenna and Sub-Millimetre Waves Section, European Space Agency, 2200 AG Noordwijk, The Netherlands (e-mail: nelson.fonseca@esa.int).

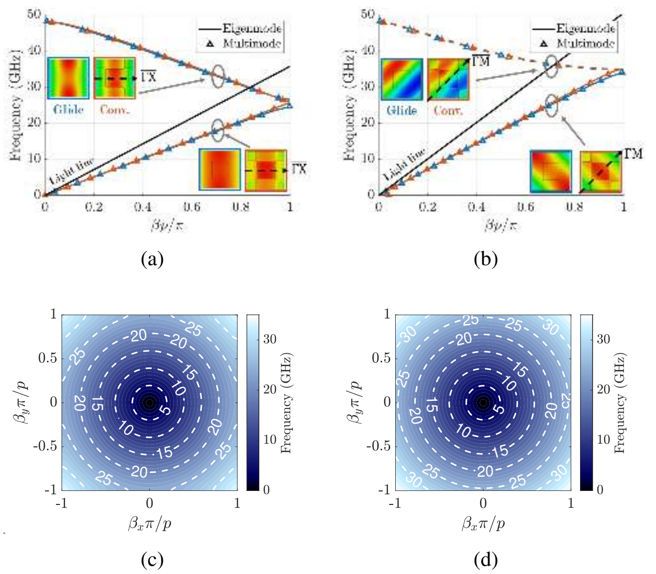

Fig. 2. Dispersion diagram for propagation along (a) $\overline{\Gamma X}$ and (b) $\overline{\Gamma M}$. The insets show the z-component of the electric field distribution in the xy-plane at $z = h/2$. 2D dispersion diagram for the (c) conventional and (d) glide-symmetric structures. The dimensions are: p = 4.2 mm, h = 2.0 mm and w = 2.2 mm.

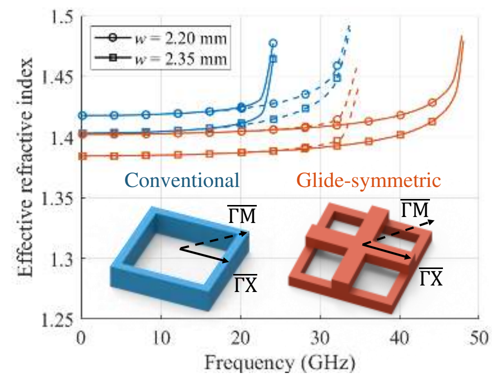

Fig. 3. Effective refractive index as a function of frequency for propagation along $\overline{\Gamma X}$ (solid lines) and $\overline{\Gamma M}$ (dashed lines) for the conventional (blue) and glide-symmetric (red) structures. The response in the $\overline{\Gamma X}$-direction in the glide-symmetric structure is obtained by mirroring the dispersion curve above the connection point in $\beta_x p = \pi$. The dimensions are: p = 4.2 mm and h = 2.0 mm.

parallel-plate waveguide (PPW) configuration (i.e. with perfect electric conductor boundary conditions at the top and bottom of the structure along the z-direction).

The structures are simulated using the multimodal transfer matrix technique described in [5], [32]–[34]. With this technique, the phase constant, effective refractive index, and dielectric losses can be obtained. The transfer matrix is obtained with the *frequency-domain solver* of *CST*. The Brillouin zones of the modal propagation constants (k_x and k_y) are then calculated using the following equation:

$$\begin{bmatrix} \mathbf{V}_3 \\ \mathbf{V}_4 \\ \mathbf{I}_3 \\ \mathbf{I}_4 \end{bmatrix} = [\mathbf{T}] \begin{bmatrix} \mathbf{V}_1 \\ \mathbf{V}_2 \\ \mathbf{I}_1 \\ \mathbf{I}_2 \end{bmatrix} = \begin{bmatrix} e^{-jk_x p}\mathbf{V}_1 \\ e^{-jk_y p}\mathbf{V}_2 \\ e^{-jk_x p}\mathbf{I}_1 \\ e^{-jk_y p}\mathbf{I}_2 \end{bmatrix} \quad (1)$$

where $\mathbf{V}_n$ and $\mathbf{I}_n$ are the voltage and current vectors of the input (1 and 2) and output (3 and 4) ports. To verify the validity of the results obtained with the multimodal analysis, the calculated phase constant is compared with the results obtained with the *eigenmode solver* of *CST*. The dispersion diagrams for the two structures are represented in Figs. 2a and 2b for the propagation along $\overline{\Gamma X}$ and $\overline{\Gamma M}$. The dielectric material has $\varepsilon_r = 2.25$ and $\tan\delta = 0.004$ and the dimensions are: p = 4.2 mm, h = 2.0 mm, and w = 2.2 mm. The multimodal results converge with the *eigenmode solver* when three modes are considered.

The stop-band between the modes in the conventional structure (blue line) is suppressed in the glide-symmetric structure (red line). From the electric field distribution in the glide-symmetric structure, it is observed that the two connected modes for propagation along $\overline{\Gamma X}$ are even with respect to the propagation direction. In fact, these connected modes are the same for propagation along $\overline{\Gamma X}$ [17]. Note that the dispersion curve for frequencies above the connection point corresponds to a higher harmonic. The dispersion curve for the fundamental mode at these frequencies is obtained through a mirroring of the dispersion curve for this harmonic with respect to $\beta_x p = \pi$. On the other hand, for propagation along $\overline{\Gamma M}$, the two modes are different. The first mode is even and the second one is odd with respect to the $\overline{\Gamma M}$-line [35]. As a result, the first mode can propagate up to 49 GHz along $\overline{\Gamma X}$ and up to 35 GHz along $\overline{\Gamma M}$ in the glide-symmetric structure. The 2D dispersion graphs, computed with the *eigenmode solver* of *CST*, for the conventional and glide-symmetric structures are presented in Figs. 2c and 2d. From the iso-frequency contours (white dashed lines) it is observed that the glide-symmetric structure is more isotropic above 20 GHz.

The effective refractive index for the propagation along $\overline{\Gamma X}$ and $\overline{\Gamma M}$ is represented in Fig. 3. The dimensions are the same as in the previous examples. As noted, the mode for propagation along $\overline{\Gamma X}$-direction in the glide-symmetric structure is obtained by mirroring the dispersion curve above the connection point with respect to $\beta_x p = \pi$. It is observed that the effective refractive index is lower in the glide-symmetric structure, compared to the conventional structure. As a result, a wider range of refractive indices can be realized with the same manufacturing accuracy. Furthermore, by tuning w so that the effective refractive indices in the two structures is the same, we observe that the bandwidth of operation is significantly wider in the glide-symmetric structure. It is noted that the same bandwidth can be obtained in the conventional structure by reducing the period. However, this comes at a cost of reduced range of realizable refractive index.

The attenuation constant is calculated with the multimodal technique and is represented in Fig. 4. No comparison is made with the eigenmode simulation since the attenuation constant cannot be retrieved with the *eigenmode solver* of *CST*. It is observed that, for dimensions that yield the same effective refractive index, the attenuation constant is approximately the same in the two structures. Nevertheless, the strong attenuation associated with the stop-band around 25 GHz for propagation

This article has been accepted for publication in a future issue of this journal, but has not been fully edited. Content may change prior to final publication. Citation information: DOI 10.1109/LAWP.2021.3092169, IEEE Antennas and Wireless Propagation Letters

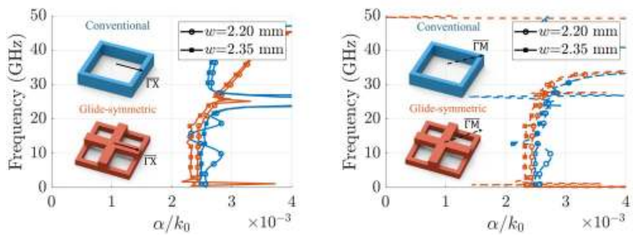

(a) (b)

Fig. 4. Simulated normalized attenuation constant for the conventional and glide-symmetric structures for propagation along (a) $\overline{\Gamma X}$, and (b) $\overline{\Gamma M}$. The dimensions are: p = 4.2 mm and h = 2.0 mm.

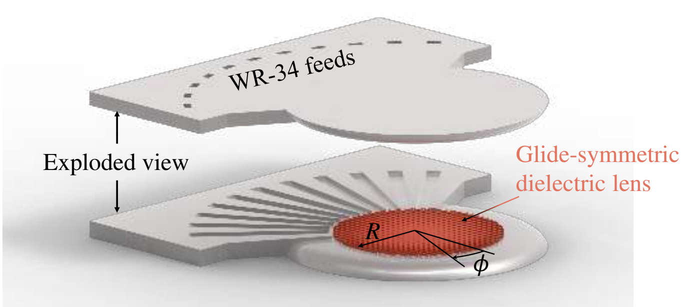

(a)

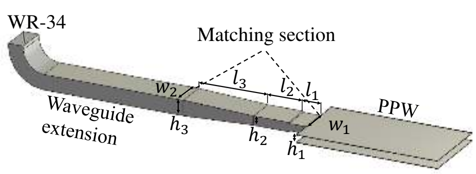

(b)

Fig. 5. (a) Illustration of the proposed Luneburg lens antenna. (b) Illustration of the feeding waveguide.

along $\overline{\Gamma X}$ in the conventional structure is not present in the glide-symmetric structure.

Next, we use the glide-symmetric dielectric structure to design a Luneburg lens operating in the K- and K_a-bands.

III. 2D Glide-Symmetric Dielectric Luneburg Lens Antenna

The Luneburg lens is a graded-index lens with rotational symmetry that transforms a spherical/cylindrical wave excited at its contour into a planar wave at the opposite side of the lens [36]. Due to the rotational symmetry, the radiation from the lens can theoretically be steered without scan losses and this beam-steering is enabled without the need of a complex feeding network. The gradient refractive index distribution for a Luneburg lens is given by

$$n(\rho) = \sqrt{2 - \left(\frac{\rho}{R}\right)^2} \quad (2)$$

where ρ is the radial position and R is the radius of the lens. At the contour of the lens, the refractive index is 1. As a result, no reflections occur at the transition between the lens and the surrounding space.

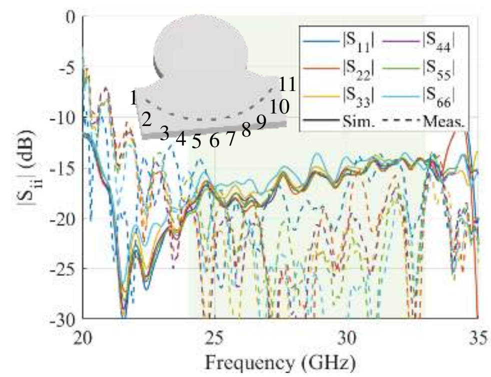

Fig. 6. Simulated (solid lines) and measured (dashed lines) reflection coefficients of ports 1-6.

A 3D-printed Luneburg lens operating from 24 to 33 GHz with radius $R = 50$ mm is implemented with the glide-symmetric dielectric structure by varying w from 0.4 mm to 2.2 mm. The realizable range of w is limited by the 3D printer. The remaining dimensions are: $p = 4.2$ mm and $h = 2.0$ mm. The lens is placed in a PPW and is fed by 11 rectangular waveguides. The assembly of the antenna is illustrated in Fig. 5a, and the feed design is illustrated in Fig. 5b. A waveguide transition is designed to match the impedance of the PPW to a WR-34 waveguide. The dimensions of the waveguide-to-PPW transition are: $h_1 = 2$ mm, $h_2 = 2.6$ mm, $h_3 = 4.32$ mm, $l_1 = 5$ mm, $l_2 = 10$ mm, $l_3 = 20$ mm, $w_1 = 8.1$ mm and $w_2 = 8.64$ mm. The waveguide feeds are extended to make room for the flanges of the coaxial-to-waveguide transitions used in the measurement of the antenna. The PPW is terminated in an exponential flare on the aperture side, providing a wideband transition to free-space propagation.

The simulated and measured reflection coefficients of the lens antenna are illustrated in Fig. 6. The measured results are time-gated to remove the effects of the coaxial-to-waveguide transition. The measurements agree well with the simulations, except for a small shift up in frequency.

The simulated and measured normalized H-plane radiation patterns at 24, 28 and 33 GHz are presented in Fig. 7. The port numbers are indicated in Fig. 6. The measured and simulated results agree well, except for slightly increased side lobe levels in the measured results. The antenna can scan 100° in the H-plane with side lobe levels below -9.5 dB and -14 dB in the measurements and simulations.

The measured 2D normalized radiation patterns at 24, 28, and 33 GHz for ports 1, 3, and 6 are illustrated in Fig. 8. The antenna produces a steerable fan-beam that is stable with frequency. In Fig. 9, the simulated and measured realized gain for ports 1-6 is represented. The gain for the remaining ports are similar due to symmetry and are omitted for clarity. Dielectric and metallic losses are included in the simulations. The measured gain is slightly lower than the simulated one, which is attributed to manufacturing errors. Importantly, the gain for the different ports is similar, which demonstrates the low scan losses in the antenna. The scan loss for $\pm 50°$ scanning is approximately 0.25 dB and 0.7 dB in the simulations

This article has been accepted for publication in a future issue of this journal, but has not been fully edited. Content may change prior to final publication. Citation information: DOI 10.1109/LAWP.2021.3092169, IEEE Antennas and Wireless Propagation Letters

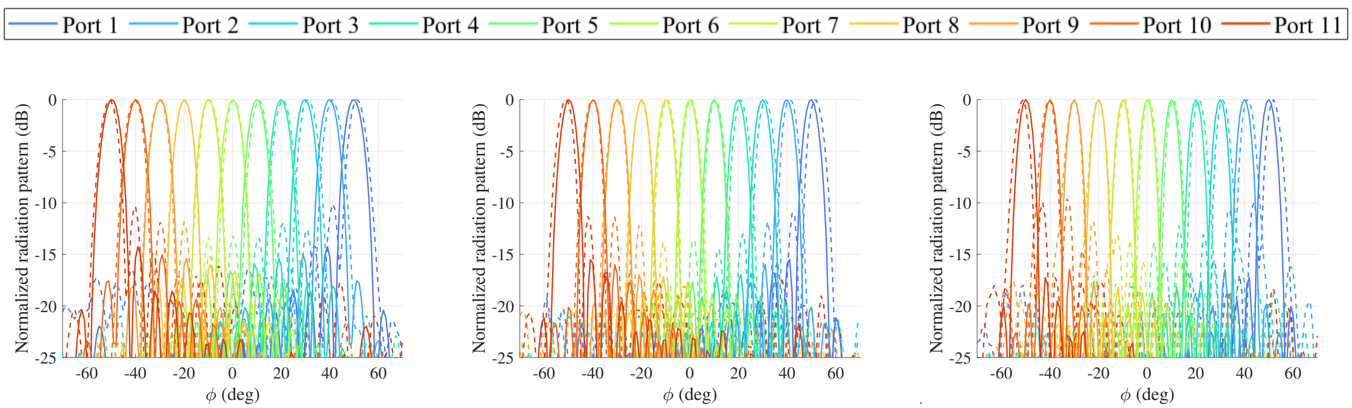

(a) (b) (c)

Fig. 7. Simulate (solid lines) and measured (dashed lines) H-plane radiation pattern at (a) 24 GHz, (b) 28 GHz, and (c) 33 GHz.

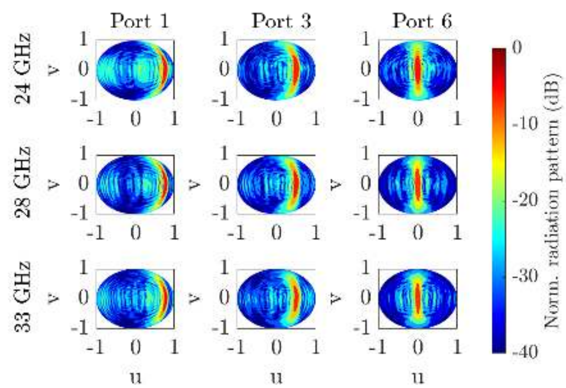

Fig. 8. Measured 2D co-polarization radiation patterns at 24, 28, and 33 GHz for ports 1, 3, and 6.

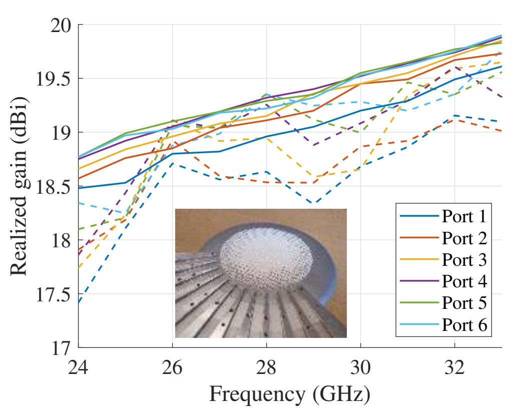

Fig. 9. Simulated (solid lines) and measured (dashed lines) realized gain of the antenna. The inset displays a photo of the prototype.

and measurements. The simulated radiation efficiency is above 70% for all frequencies and ports.

In Tab. I, the proposed lens antenna is compared with reported wide-scanning planar lens antennas operating at K and K_a-band. It is noted that, due to the dielectric losses, the proposed antenna has slightly lower simulated radiation efficiency than fully-metallic antennas. However, the proposed antenna is more compact and can be 3D printed, which results in a low manufacturing cost.

TABLE I
REPORTED WIDE-SCANNING 2D LENS ANTENNAS

Ref.	Rel. BW	Height/Radius	Rad. eff.	Manufacturing
[19]	21%	0.05	> 80%	Milling
[27]	25%	0.25	> 90%	Milling
[28]	42%	0.17	> 90%	Milling
[29]	29%	0.15	> 85%	Milling
[30]	29%	0.15	> 75%	Milling
[31]	21%	0.09	> 80%	Printed technology
This work	31%	0.04	> 70%	3D printing

IV. CONCLUSION

In this letter, we proposed and studied a dielectric 2D periodic structure with glide symmetry. The dielectric structure is covered in the top and bottom with metal, in a PPW configuration. We demonstrated that glide symmetry provides a lower minimum realizable effective refractive index, increased isotropy, and wider operational bandwidth, compared to the a conventional periodic structure. These features are advantageous for the design of dielectric lens antennas that can be manufactured using additive manufacturing. We used the proposed glide-symmetric structure to design a 2D Luneburg lens antenna operating in the K- and K_a bands. The designed antenna produces a directive fan-beam that can be steered 100° with negligible scan losses in the H-plane. These properties are attractive to produce low-cost multiple beam antennas for 5G/6G base stations and SATCOM user terminals.

ACKNOWLEDGEMENT

The authors would like to thank the *Premix group* for supplying the filaments used for the manufacturing of the lens.

This article has been accepted for publication in a future issue of this journal, but has not been fully edited. Content may change prior to final publication. Citation information: DOI 10.1109/LAWP.2021.3092169, IEEE Antennas and Wireless Propagation Letters

REFERENCES

[1] P. J. Crepeau and P. R. McIsaac, "Consequences of symmetry in periodic structures," *Proc. IEEE*, vol. 52, no. 1, pp. 33–43, Jan 1964.

[2] A. Hessel, M. H. Chen, R. C. M. Li, and A. A. Oliner, "Propagation in periodically loaded waveguides with higher symmetries," *Proc. IEEE*, vol. 61, no. 2, pp. 183–195, Feb 1973.

[3] R. Mittra and S. Laxpati, "Propagation in a wave guide with glide reflection symmetry," *Can. J. Phys.*, vol. 43, no. 2, pp. 353–372, 1965.

[4] R. Kieburtz and J. Impagliazzo, "Multimode propagation on radiating traveling-wave structures with glide-symmetric excitation," *IEEE Trans. Antennas Propag.*, vol. 18, no. 1, pp. 3–7, Jan 1970.

[5] O. Quevedo-Teruel, Q. Chen, F. Mesa, N. J. G. Fonseca, and G. Valerio, "On the benefits of glide symmetries for microwave devices," *IEEE Journal of Microwaves*, vol. 1, no. 1, pp. 457–469, 2021.

[6] M. Ebrahimpouri, O. Quevedo-Teruel, and E. Rajo-Iglesias, "Design guidelines for gap waveguide technology based on glide-symmetric holey structures," *IEEE Microw. Wireless Compon. Lett.*, vol. 27, no. 6, pp. 542–544, June 2017.

[7] M. Ebrahimpouri, E. Rajo-Iglesias, Z. Sipus, and O. Quevedo-Teruel, "Cost-effective gap waveguide technology based on glide-symmetric holey EBG structures," *IEEE Trans. Microw. Theory Techn.*, vol. 66, no. 2, pp. 927–934, Feb 2018.

[8] A. Vosoogh, H. Zirath, and Z. S. He, "Novel air-filled waveguide transmission line based on multilayer thin metal plates," *IEEE Trans. THz Sci. Techn.*, vol. 9, no. 3, pp. 282–290, May 2019.

[9] M. Ebrahimpouri, A. A. Brazalez, L. Manholm, and O. Quevedo-Teruel, "Using glide-symmetric holes to reduce leakage between waveguide flanges," *IEEE Microw. Wireless Compon. Lett.*, vol. 28, no. 6, pp. 473–475, June 2018.

[10] Z. He, S. An, J. Liu, and C. Jin, "Variable high precision wide D-band phase shifter," *IEEE Access*, 2020.

[11] A. Monje-Real, N. J. G. Fonseca, O. Zetterstrom, E. Pucci, and O. Quevedo-Teruel, "Holey glide-symmetric filters for 5G at millimeter-wave frequencies," *IEEE Microw. Wireless Compon. Lett.*, vol. 30, no. 1, pp. 31–34, Jan 2020.

[12] M. Ebrahimpouri and O. Quevedo-Teruel, "Ultrawideband anisotropic glide-symmetric metasurfaces," *IEEE Antennas Wireless Propag. Lett.*, vol. 18, no. 8, pp. 1547–1551, Aug 2019.

[13] A. Alex-Amor, F. Ghasemifard, G. Valerio, M. Ebrahimpouri, P. Padilla, J. M. Fernandez-Gonzalez, and O. Quevedo-Teruel, "Glide-symmetric metallic structures with elliptical holes for lens compression," *IEEE Trans. Microw. Theory Techn.*, pp. 1–1, 2020.

[14] A. Demetriadou and Y. Hao, "A grounded slim Luneburg lens antenna based on transformation electromagnetics," *IEEE Antennas Wireless Propagat. Lett.*, vol. 10, pp. 1590–1593, 2011.

[15] Q. Chen, F. Giusti, G. Valerio, F. Mesa, and O. Quevedo-Teruel, "Anisotropic glide-symmetric substrate-integrated-holey metasurface for a compressed ultrawideband Luneburg lens," *Appl. Phys. Lett.*, vol. 118, no. 8, p. 084102, 2021.

[16] M. Ebrahimpouri, L. F. Herran, and O. Quevedo-Teruel, "Wide-angle impedance matching using glide-symmetric metasurfaces," *IEEE Microw. Wireless Compon. Lett.*, vol. 30, no. 1, pp. 8–11, 2020.

[17] O. Quevedo-Teruel, M. Ebrahimpouri, and M. N. M. Kehn, "Ultrawideband metasurface lenses based on off-shifted opposite layers," *IEEE Antennas Wireless Propag. Lett.*, vol. 15, pp. 484–487, Dec 2016.

[18] T. Chang, J. U. Kim, S. K. Kang, H. Kim, D. K. Kim, Y.-H. Lee, and J. Shin, "Broadband giant-refractive-index material based on mesoscopic space-filling curves," *Nat. Commun.*, vol. 7, Article number 12661, 2016.

[19] O. Quevedo-Teruel, J. Miao, M. Mattsson, A. Algaba-Brazalez, M. Johansson, and L. Manholm, "Glide-symmetric fully metallic Luneburg lens for 5G communications at Ka-band," *IEEE Antennas Wireless Propag. Lett.*, vol. 17, no. 9, pp. 1588–1592, Sept 2018.

[20] P. Bantavis, C. G. Gonzalez, R. Sauleau, G. Goussetis, S. Tubau, and H. Legay, "Broadband graded index Gutman lens with a wide field of view utilizing artificial dielectrics: a design methodology," *Opt. Express*, vol. 28, no. 10, pp. 14 648–14 661, May 2020.

[21] P. Arnberg, O. Barreira Petersson, O. Zetterstrom, F. Ghasemifard, and O. Quevedo-Teruel, "High refractive index electromagnetic devices in printed technology based on glide-symmetric periodic structures," *Appl. Sci.*, vol. 10, no. 9, 2020.

[22] D. Cavallo and C. Felita, "Analytical formulas for artificial dielectrics with nonaligned layers," *IEEE Trans. Antennas Propag.*, vol. 65, no. 10, pp. 5303–5311, Oct 2017.

[23] D. Cavallo, "Dissipation losses in artificial dielectric layers," *IEEE Trans. Antennas Propag.*, vol. 66, no. 12, pp. 7460–7465, Dec 2018.

[24] Z. Sipus and M. Bosiljevac, "Modeling of glide-symmetric dielectric structures," *Symmetry*, vol. 11, no. 6, 2019.

[25] D. Jia, Y. He, N. Ding, J. Zhou, B. Du, and W. Zhang, "Beam-steering flat lens antenna based on multilayer gradient index metamaterials," *IEEE Antennas Wireless Propag. Lett.*, vol. 17, no. 8, pp. 1510–1514, Aug 2018.

[26] F. Doucet, N. J. G. Fonseca, E. Girard, H. Legay, and R. Sauleau, "Analytical model and study of continuous parallel plate waveguide lens-like multiple-beam antennas," *IEEE Trans. Antennas Propag.*, vol. 66, no. 9, pp. 4426–4436, Sept. 2018.

[27] Q. Liao, N. Fonseca, and O. Quevedo-Teruel, "Compact multibeam fully metallic geodesic Luneburg lens antenna based on non-Euclidean transformation optics," *IEEE Trans. Antennas Propag.*, vol. 66, no. 12, pp. 7383–7388, Dec. 2018.

[28] H. Lu, Z. Liu, Y. Liu, H. Ni, and X. Lv, "Compact air-filled Luneburg lens antennas based on almost-parallel plate waveguide loaded with equal-sized metallic posts," *IEEE Trans. Antennas Propag.*, vol. 67, no. 11, pp. 6829–6838, Nov. 2019.

[29] N. J. G. Fonseca, Q. Liao, and O. Quevedo-Teruel, "Equivalent planar lens ray-tracing model to design modulated geodesic lenses using non-euclidean transformation optics," *IEEE Trans. Antennas Propag.*, vol. 68, no. 5, pp. 3410–3422, May 2020.

[30] N. J. G. Fonseca, Q. Liao, and O. Quevedo-Teruel, "Compact parallel-plate waveguide half-Luneburg geodesic lens in the Ka-band," *IET Microw. Antennas Propag.*, vol. 15, no. 2, pp. 123–130, Feb. 2021.

[31] O. Zetterstrom, R. Hamarneh, and O. Quevedo-Teruel, "Experimental validation of a metasurface Luneburg lens antenna implemented with glide-symmetric substrate-integrated-holes," *IEEE Antennas Wireless Propag. Lett. (early access)*, 2021.

[32] M. Bagheriasl, O. Quevedo-Teruel, and G. Valerio, "Bloch analysis of artificial lines and surfaces exhibiting glide symmetry," *IEEE Trans. Microw. Theory Techn.*, vol. 67, no. 7, pp. 2618–2628, 2019.

[33] M. Bagheriasl and G. Valerio, "Bloch analysis of electromagnetic waves in twist-symmetric lines," *Symmetry*, vol. 11, no. 5, 2019.

[34] F. Mesa, G. Valerio, R. Rodriguez-Berral, and O. Quevedo-Teruel, "Simulation-assisted efficient computation of the dispersion diagram of periodic structures: A comprehensive overview with applications to filters, leaky-wave antennas and metasurfaces," *IEEE Antennas Propag. Mag. (early access)*, 2021.

[35] Q. Chen, F. Mesa, X. Yin, and O. Quevedo-Teruel, "Accurate characterization and design guidelines of glide-symmetric holey EBG," *IEEE Trans. Microw. Theory Techn*, vol. 68, no. 12, pp. 4984–4994, 2020.

[36] R. Luneburg, "Mathematical theory of optics," *Brown University Press, Providence, RI*, pp. 208–213, 1944.